lubricants

MDPI

Article

Experimental Investigation of a Highly Loaded Half-Journal Bearing

James Layton, Humberto Medina, Hasna Fadhila, Benjamin C. Rothwell *, Stephen Ambrose, Katrina Farbrother and Carol Eastwick

Mechanical and Aerospace Systems Research Centre, The University of Nottingham, Nottingham NG7 2TU, UK
* Correspondence: benjamin.rothwell@nottingham.ac.uk

Abstract

A dedicated experimental rig is presented for a half-journal bearing operating under highly loaded, well-controlled hydrodynamic lubrication conditions relevant to turbomachinery. The apparatus combines pressure measurements in the film, distributed temperature measurements in the shaft and bush, and ultrasonic film-thickness measurements that map the circumferential film-thickness profile across the lubrication region. Experiments are reported for normal loads of 5–20 kN and shaft speeds of 1000–4000 rpm with controlled oil supply conditions. The measured pressure and temperature trends are consistent with established hydrodynamic lubrication behaviour. The film thickness measurements confirm full-film operation across the tested operating envelope, while indicating increased uncertainty in regions affected by cavitation. A correlation for the temperature rise due to viscous heating is proposed as a compact representation of the data. The rig design and accompanying measurements provide a benchmark-quality data set intended for validation and development of thermal elasto-hydrodynamic lubrication (TEHL)/computational fluid dynamics (CFD) models under high load and speed conditions.

Keywords: half-journal; hydrodynamic lubrication; film thickness; ultrasonic measurement; thermal response

1. Introduction and Background

In many industries, highly loaded lubricated contacts are employed as an integral part of mechanical system design. These systems may include components such as journal bearings, meshing gear pairs, and rolling element bearings. Proper lubrication reduces friction and wear during operation. This leads to increased energy efficiency, improved reliability, and extended component lifetime, while simultaneously reducing maintenance intervals and operating costs. Furthermore, lubrication fluids are commonly used as part of thermal management in mechanical systems. By cooling key components, lubrication helps prevent heat-related failure and improves overall system performance. Thus, improved lubrication systems are increasingly important for industries seeking environmentally and economically sustainable solutions, such as the transition to sustainable aviation fuels (SAFs) in aerospace engines and the increased availability of renewable energy sources, including wind turbine technology.

Developing industrial technology under increasingly extreme operating conditions requires greater performance from its lubricated components. The lubrication performance is a multiphysics problem that is dependent on several variables, including operating conditions, lubricant rheology, material properties, and surface finishes. Optimising the

Check for updates

Received: 24 October 2025
Revised: 28 January 2026
Accepted: 30 January 2026
Published: 6 February 2026

Copyright: © 2026 by the authors. Licensee MDPI, Basel, Switzerland. This article is an open access article distributed under the terms and conditions of the Creative Commons Attribution (CC BY) license.

performance of lubricated components is a key factor in maximising energy efficiency. High-quality experimental data are required to support the development of theoretical and modelling capabilities to improve lubrication performance in industry.

Lubricated components, such as journal bearings, are often designed to operate hydrodynamically, where the relative motion of the adjacent bodies drives the lubricant into a converging-diverging gap, separating the surfaces. The separation of the surfaces by this oil film produces the desired reduction in friction and wear, and the performance of this lubrication is dependent on the pressure field that develops within the film. This pressure field is commonly described using the Reynolds equation and coupled to the elastic deformation of the surfaces as well as to temperature changes, which are fundamental to thermal elasto-hydrodynamic lubrication (TEHL) theory within the field of tribology. To validate and enhance the capability of TEHL modelling theory in modern contexts, it is necessary to have a robust experimental methodology, well-defined boundary conditions, and a broad experimental data set. The lubricating film is thin, typically <100 μm thick, creating challenges both for numerical models and experimental investigations.

Experimental investigations continue to be important for developing numerical models for lubricating films and must provide robust and accurate data for validation. Computational models for bearing designs rely on high-quality experimental data sets for verifying the accuracy of pressure distribution and load-carrying capacity in liquid-lubricated bearings, e.g., in the design of conical bearings in [1]. Experimental investigation into the influence of operational parameters such as rotational speed and supply pressure can also assist in the verification of numerical models, e.g., Ref. [2] on an aerostatic bearing-rotor system and Ref. [3] on spiral-groove thrust bearings. Well-defined conditions at the boundaries are also an important factor in developing and validating numerical models.

The first experiments on lubricated contacts were by [4] who immersed a bearing in an oil bath at constant temperature to investigate the frictional resistances under fully lubricated conditions. The bearing had a half-journal configuration where a shaft of diameter 100 mm rotated within a bush that spans 180° of the circumference. The coefficient of friction, measured with a lever and pointer mechanism, was found to increase with increasing rotational speed but decrease with increasing load. Tower's experiments provided evidence of a fully formed film separating the contacting surfaces in a hydrodynamic lubrication regime.

An experimental rig developed by [5] used a fully cylindrical bush in a study to measure the circumferential pressure distribution under full-film lubrication conditions. A single hole in the bush was used to measure the pressure in the oil film at different angular positions. The temperature of the oil was measured from a single position by installing a thermojunction in the pressure hole. The experiments were run with four types of oil, obtaining the pressure profiles and coefficients of friction, with the eccentricity and attitude angle estimated from the pressure profiles. The maximum pressure observed in the results was 54 MPa.

Ma et al. [6] built a two-axial-groove journal bearing experimental rig with a shaft diameter of 110 mm for investigating thermal effects in circular and elliptical bearings. Thermocouples were installed 0.75 mm below the bush surface along both the circumferential and axial directions. The maximum load and rotational speed in the experiment were 33 kN and 7000 rpm, respectively. The results showed that the temperature variation was more significant along the circumference than in the axial direction.

Syverud et al. [7] investigated the effect of heating or cooling of a journal bearing shaft. The load was applied on a floating bush with nine thermocouples embedded along the mid-plane to measure the circumferential temperature. The shaft was supported by two pre-loaded ball bearings with a diameter of 100 mm and a clearance with the bush of

70 μm. The shaft contained an internal oil system with controlled flow rate and temperature at either 100 °C or 50 °C, providing either heating or cooling. The bearing load and shaft rotational speed were 3000 and 1750 rpm, respectively.

Ferron et al. [8] used a journal bearing test rig to compare experimental temperature results with a numerical model. A steel journal with a diameter of 100 mm was placed within a bronze bush with a radial clearance of 145 μm. Thermocouples were installed 0.5 mm below the surface along the circumference of the bush, and pressure was measured through 15 holes in the bush. Proximity sensors monitored the shaft position, which was used to estimate the eccentricity of the shaft. Fresh oil was supplied to the bearing in a single axial groove. The test rig was subsequently used in multiple experimental investigations. Ref. [9] used the apparatus from [8] to investigate the effect of groove location and supply pressure on the journal bearing performance. The groove position was varied between ±30° from top dead centre, which showed changes in the maximum temperature and pressure. The maximum load and rotational speed were 8 kN and 4000 rpm, respectively. Ref. [10] changed the test rig to a two-axial groove journal bearing and investigated the influence of supply temperature and supply pressure. They found that the supply temperature only affected the oil flow rate, and the supply pressure affected both the flow rate and film thickness.

Ultrasonic methods are robust for film thickness measurements of lubricant films because the procedure is non-invasive, non-destructive, and does not require transparent materials. Ref. [11] developed an ultrasonic method for measuring the thickness of lubricating films in bearing systems using the signal reflected by the interfaces with the film. The methodology is applied to an elasto-hydrodynamic lubricant film and recorded film thickness values in the range of 50–500 nm. An ultrasonic method was applied by [12] to measure the oil film thickness in a journal bearing. The experimental rig uses a steel shaft and brass bush with a diametrical clearance of 50 μm, with a maximum load and rotational speed of 8.8 kN and 710 rpm. A single transducer is placed at the bottom-dead-centre of the bearing to measure the film thickness at one position, which is shown to compare well with published numerical results. Ref. [13] used the ultrasonic method to measure the oil film thickness in a journal bearing. The diameter of the shaft was 75 mm with a clearance with the bush of 25 μm. The maximum applied load and rotational speed were 10 kN and 800 rpm, respectively. The transducer was installed in the shaft to take measurements along the circumference during operation. The results showed good comparison of the experimental film thickness profile with mathematical solutions, particularly in the converging region. However, the signal was shown to be disrupted by cavitation in the oil film.

A test rig was used in [14] to determine the static equilibrium position in hydrodynamic journal bearings and compare it with numerical results. Two eddy current proximity sensors were used to measure the position of a shaft with a diameter of 25 mm and a radial clearance with a bush of 210 μm. This gives an X and Y coordinate position for the shaft. A rotational speed range of 250–3000 rpm was used with the primary load being the weight of the shaft, approximately 0.5 kg.

Marey et al. [15] used a journal bearing facility to investigate the effect of oil supply pressure on the film pressure and temperature profiles. The shaft diameter was 104.97 mm with a radial clearance with the bush of 52 μm, and oil was supplied through a circumferential groove in the bush. Relatively slow rotational speeds were tested, with a maximum speed of 102 rpm, and the maximum load was approximately 6 kN. The results showed that lubrication performance was impacted by a drop in the supply pressure of 25%.

Van Der Meer et al. [16] used a hydrodynamic journal bearing rig to measure the transition speed from a mixed to a full lubrication regime using a magnetorheological

fluid. A shaft with a diameter of 50 mm supported by two ball bearings was driven by a 5.5 kW AC electric motor in a stationary bush with a constant radial load applied. Friction measurements were taken with a moment arm, and oil was supplied through two inlet holes in the bush at ±90 °C. Rotational speed varied from 0 to 500 rpm with an applied load of 2.5 kN.

Cao et al. [17] built an experimental facility to investigate the thermohydrodynamic performance of a steadily loaded hybrid journal bearing. The supply flow rate, external load, inlet pressure, centreline pressure, and temperature distribution along the bush surface were measured in a parametric study with a maximum rotational speed of 2200 rpm and a maximum load of approximately 5 kN.

The influence of the oil supply conditions has been shown in several studies to significantly impact the lubrication performance in film bearings, underscoring the need for well-defined boundary conditions for validating numerical models of lubrication films. Additionally, most existing experimental studies operate under normal loads below 10 kN and typically lack data sets that simultaneously capture pressure, temperature, and film thickness behaviour across a wide range of operating parameters. This gap limits the ability to validate models under high-load, fully characterised conditions.

To address this need, the present study introduces an experimental rig featuring a unique implementation of a half-journal geometry with a distinctive instrumentation layout, open half-journal access, and boundary-condition control. The aim is to investigate the behaviour of hydrodynamically lubricated films under a wide range of controlled conditions and report key measurements, which are pressure in the film, temperature distribution in the bush, and the thickness of the oil film. The open setup of the rig offers greater control of the inlet conditions, facilitates visualisation of the exiting flow, and allows for well-defined boundary conditions.

One oil lubricant (Eastman Turbo Oil 2197) is used in the experiments reported here. Cross-lubricant comparison is beyond the scope of this study. Measurements from operating conditions under a shaft rotational speed of 1000–4000 rpm and a normal load of 5–20 kN are reported. This study will serve as an experimental platform and provide a data set for high-load validation to support developing numerical models.

2. Experimental Method

2.1. Rig Configuration and Capability

The experimental rig is designed to enhance understanding of fluid flow in journal bearings and provide data for validation of computational models. The rig uses a half-journal bearing to decouple inlet/outlet recirculation relative to a full journal, enabling better control of inlet conditions, facilitating visualisation of exit flow, and supporting validation workflows by providing clearer boundaries. This will support ongoing CFD and TEHL modelling developments by providing validation-oriented data sets and is capable of operating with varied oil flow rates, shaft speeds, temperatures, and load conditions typical in many engineering applications. It is housed within a facility at the Mechanical and Aerospace Systems (MAS) Research Centre at the University of Nottingham. The facility allows test units to be rapidly developed and connected to a drive stand with control, data acquisition, and safety systems already in place. A schematic of the facility is shown in Figure 1 and a photo of the experimental rig is shown in Figure 2. A drawing of the half-journal schematic in the experimental rig is also shown in Figure 2 with the major elements of the setup labelled. The parameters of the half-journal bearing are described later in Section 2.1.2.

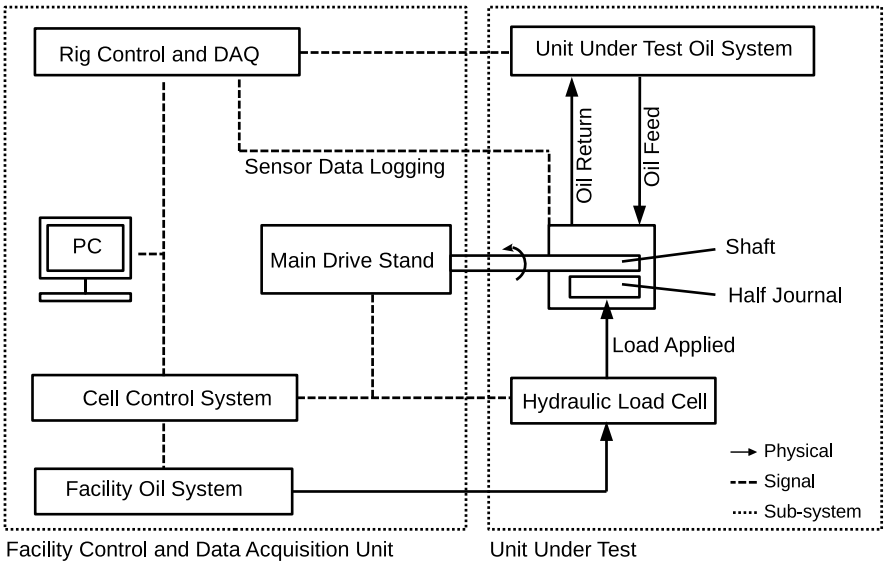

Figure 1. Schematic of the experimental facility.

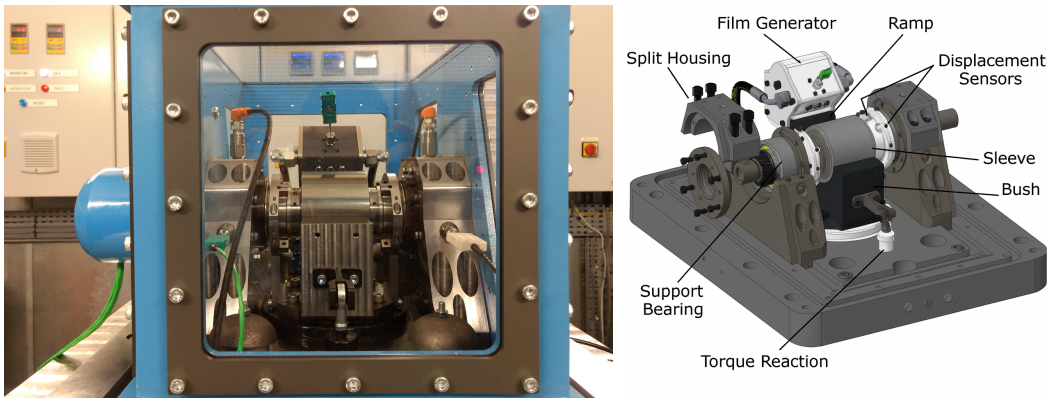

(**a**) (**b**)

Figure 2. (**a**) Photo of the half-journal in the experimental rig; (**b**) a schematic showing the major elements.

2.1.1. Facility Control and Data Acquisition Unit

The main drive stand consists of a 3-phase AC motor connected to an orbital gear system, which provides output shaft speeds of up to 15,000 rpm and has a power rating of 138 kW, with a maximum torque of 440 Nm.

The facility has an independent oil system used to provide oil to the gearbox of the drive stand and to a hydrostatic system for the hydraulic load cell. The hydraulic load cell is used to apply the external load with axial symmetry. Oil is subsequently scavenged from the load system through four lines into a common manifold and returned to the tank by the scavenge pump. This allows us to operate the facility systems independently of any requirements for the Unit Under Test.

All control and monitoring signals are safely processed in a control room using a single PC, which is also used for data acquisition of all the recorded channels. Specific details of the instrumentation and recorded data are provided in Section 2.2.

2.1.2. Unit Under Test (UUT) and Bearing Parameters

The Unit Under Test (UUT) consists of a half-journal configuration, made up of an instrumented shaft and bush, which are contained within a chamber at ambient pressure. Both components are made from EN24T with a surface finish of Ra 0.1. A cross-sectional schematic of the UUT is provided in Figure 3.

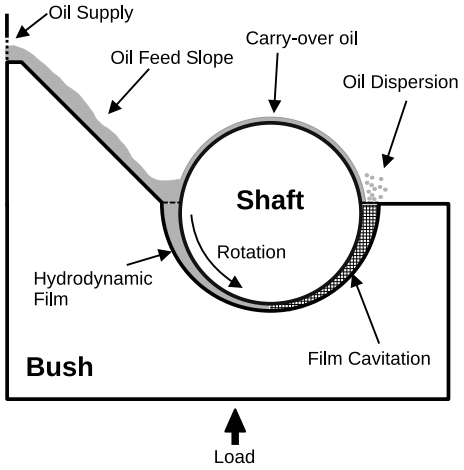

Figure 3. Schematic of the half-journal experimental rig during operation.

The instrumented shaft is supported by two cylindrical roller bearings 230 mm apart. The half journal is 100.2 mm in diameter, providing a nominal 100 µm radial clearance between the shaft and bush (at zero load). Both shaft and bush are manufactured within a tolerance of 0.01 mm. In order to provide hydrodynamic lubrication to the clearance gap, oil is supplied through an inlet film generator as shown in Figure 3. The flow rate of the supplied oil can be controlled by the operator and is set to a sufficiently high value to ensure hydrodynamic lubrication is always achieved. A single feed pump in the UUT oil system can supply oil at 0–50 L/min to the rig from the UUT oil system tank, which is maintained at 30 °C by a cartridge heater. Preliminary testing was conducted to determine the required flow rates for the conditions tested, and it was found that for the highest rpm, a flow rate of 20 L/min was used. Oil drains from the rig under gravity and is returned to the UUT oil system tank by a scavenge pump.

2.1.3. Lubricant Properties

Only one lubricant (Eastman Turbo Oil 2197) is used in this experimental test rig. Cross-lubricant comparison and a lubricant performance study are beyond the scope of this paper. The key lubricant property information is publicly available from [18] and reiterated here for ease of replication. The reported density of the oil at 15 °C is 0.9968 kg. The kinematic viscosity at 40 °C is 26.98 mm^2/s, while the kinematic viscosity at 100 °C is 5.28 mm^2/s. This oil is chosen because it is commonly used in aerospace applications due to its suitability for high-temperature environments.

2.2. Instrumentation, Error, and Uncertainty

2.2.1. Temperature and Pressure Measurement

The rig is equipped with 20 standard K-type thermocouples and 6 pressure tappings, as shown in Figure 4, to monitor the temperature and pressure of the lubricating film at multiple points across the film region. These thermocouples, which are class 2 tolerance with a manufacturer-stated accuracy of ±2.5 °C for temperatures ranging from −40 °C to +333 °C, provide reliable temperature measurements. The thermocouples are embedded 1 mm within the shaft/bush material (as shown schematically) and therefore

measure a near-surface solid temperature rather than the direct oil temperature. The temperatures reported here are steady, time-averaged values; therefore, the transient effects of the inertia of the bushing material's thermal conductivity are filtered by the material.

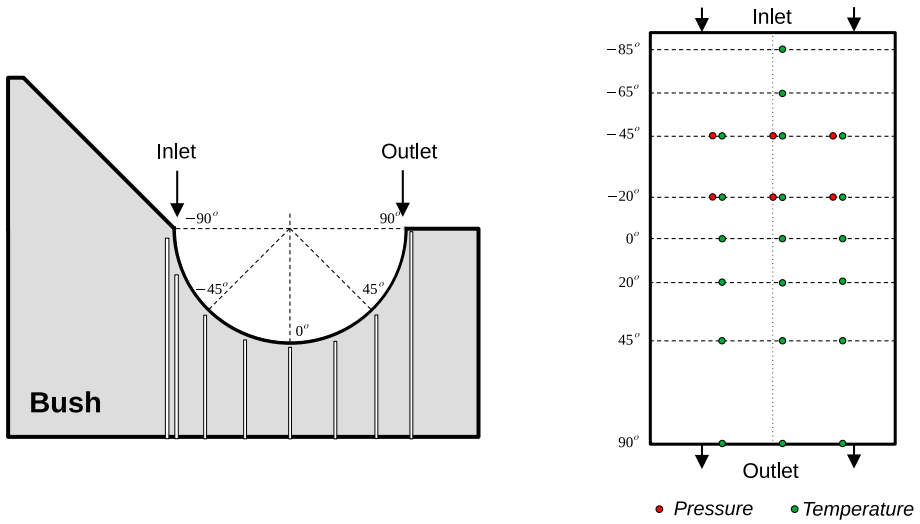

Figure 4. Embedded sensor positions in the bush. The thermocouples are embedded 1 mm within the bush material. (**a**) Side view; (**b**) Top view.

By comparing the centreline and off-centre temperature profiles of two extreme sample cases in Figure 5, consistent temperature readings are obtained across the axial range. The maximum standard deviation recorded across all tested conditions, considering all sensors, was 0.25 K. Therefore, even under the most conservative scenario, the maximum error estimated in the temperature measurements is only 3%, ensuring a high level of accuracy in the data collected.

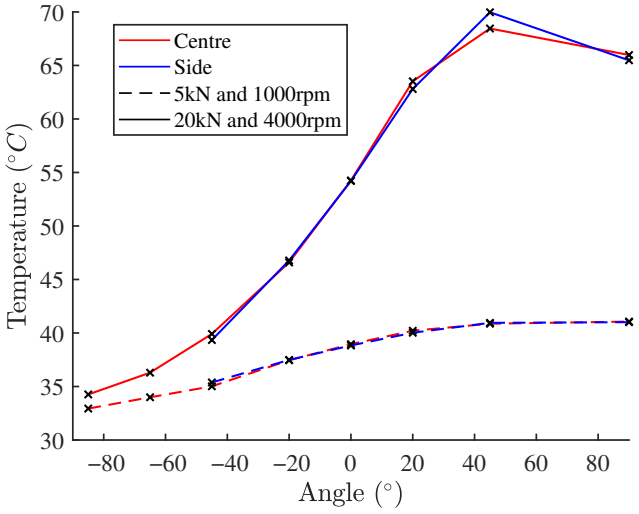

Figure 5. Comparison of the centre-line and off-centre temperature profiles.

Pressure is monitored using STS (Sensor Technik Sirnach) 133209 ATM 1ST sensors (anufacturer: STS Sensor Technik Sirnach AG, Sirnach, Switzerland) with an accuracy of ±0.1% in the range of 0–10 V DC, corresponding to a pressure range of 0–200 bar. The confidence interval is calculated such that 95% of the data lies within ±0.9534 bar. At full scale, this produces an estimated error of ±1.1534 bar.

2.2.2. Film Thickness Measurement

The rig utilises ultrasonic sensors to measure film thickness across angular positions between -90° and 90° from the bottom dead centre, allowing comprehensive monitoring of the film thickness profile across the half-journal bearing under various operating conditions. The measurement technique uses amplitude and phase-change methods, as well as resonant dip techniques, to obtain the circumferential film thickness profiles. The theoretical principles are well understood and have been presented in the literature. The reader is referred to [11,19] for further details on the acquisition methodology. The method has been validated in various lubricated contact configurations, as summarised in the review in [20].

The novelty of the setup is the integration of the ultrasonic measurements with instrumented pressure and temperature measurements in a high-load half-journal platform with controlled inlet conditions. This capability is enabled by a bespoke, commercially provided arrangement using ultrasonic techniques, where two ultrasonic sensors are mounted on the shaft to emit a signal through the lubricating film. The film thickness is determined by analysing the characteristics of the reflected signal using a proprietary algorithm by Tribosonics LTD (Sheffield, UK).

The method's suitability was initially verified by measuring a known lubricated gap height in a stationary setup, with results showing a deviation of less than 2.1 µm from the set height. The maximum standard deviation recorded in the current work further confirms the precision and repeatability provided by the ultrasonic measurement system.

2.2.3. Angular Position and Drive Characterisation

Angular position is measured using a radial magnetic ring, RLS MR050E. This was installed as per the manufacturer's guidelines and, as such, has a maximum installation error of 0.08°. Additional errors arise from the accuracy of the magnet (estimated as 0.1° for the 50 mm diameter ring) and the 0.04° reading error, giving a total estimated error of 0.22°.

The shaft is driven by a 138 kW motor with a maximum speed of 15,000 rpm. For the tests conducted in this study, the maximum shaft speed used was 4000 rpm. Based on a previous characterisation of the drive by [21], the estimated uncertainty of the set point is ± 4 rpm. This gives an estimated maximum uncertainty of 0.8% for the range of tests conducted.

2.3. Test Matrix

The experimental test parameters include the shaft rotational speed and the applied load. The shaft rotational speed is varied in the range 1000–4000 rpm in intervals of 500 rpm, and the applied load is varied in the range 5–20 kN in intervals of 2.5 kN. This range was selected to ensure both the stability of the bearing and that the conditions were well within the operating range for the rig. The complete test matrix is presented in Figure 6. Oil flow rates were prescribed to ensure that all experimental tests were conducted within the hydrodynamic lubrication regime. It was observed during operation that all of the oil did not enter the bearing test region, but some overflowed into the surrounding chamber.

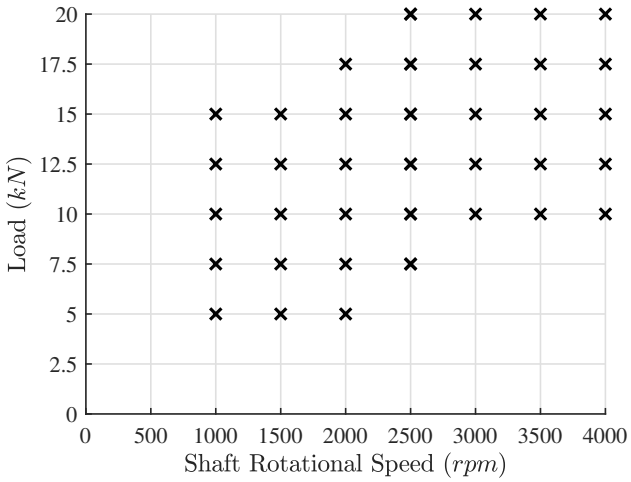

Figure 6. Experimental test matrix.

3. Results and Discussion

Experiments were performed across an applied normal load range of 5–20 kN and a shaft rotational speed range of 1000–4000 rpm. The experimental measurements include pressure in the film, temperature in the bush near the interface with the lubricating oil, and measurements of the film thickness using ultrasonic signals. This section presents the results of the experimental investigation, which includes the measurements of each variable against the experimental parameters. The pressure measurements are presented as axial profiles at the angular locations of $-45°$ and $-20°$. A predictive maximum temperature methodology is developed using a logarithmic model to estimate the temperature rise in a half-journal configuration based on the operational load and rotational speed. Analysis of the film height profiles highlights the trend with the variation of load and rotational speed.

Figure 7 shows the axial profiles of pressure measured at the $-45°$ and $-20°$ locations from the bottom-dead-centre (BDC) of the lubrication region. There is a clear and consistent pressure rise between the $-45°$ and $-20°$ angular locations as expected from lubrication theory, where the pressure increases as the fluid is driven into the converging gap formed between the shaft and bush. The gradient in pressure between the $-45°$ and $-20°$ locations tends to increase with the applied load; for example, in Figure 7a the change in pressure between the angular positions along the centreline is approximately 0.5 MPa at 5 kN and 2 MPa at 15 kN. The pressure measurements do not capture the peak value or the full circumferential profile; the reduced pressure tappings, in particular around the minimum film height, will minimise the distribution to the film. A trend in the pressure between the two angular positions is observable from the results and offers an opportunity for numerical model validation with minimal distribution to the film and therefore lubrication performance.

Comparison of the axial profiles shows a consistent symmetry about the centreline of the bearing at axial position 37.5 mm. The off-centreline pressure tappings are generally within 2% agreement with each other, with a mean difference of approximately 0.25 MPa, demonstrating there is good alignment between the shaft and bush during operation. Similar to the centreline gradients, the gradient between the central and off-centre pressure measurements increases with the applied load and is consistently greater at the $-20°$ location. This pattern further highlights agreement with lubrication theory, where the pressure profile becomes more focused on the peak value with increasing load.

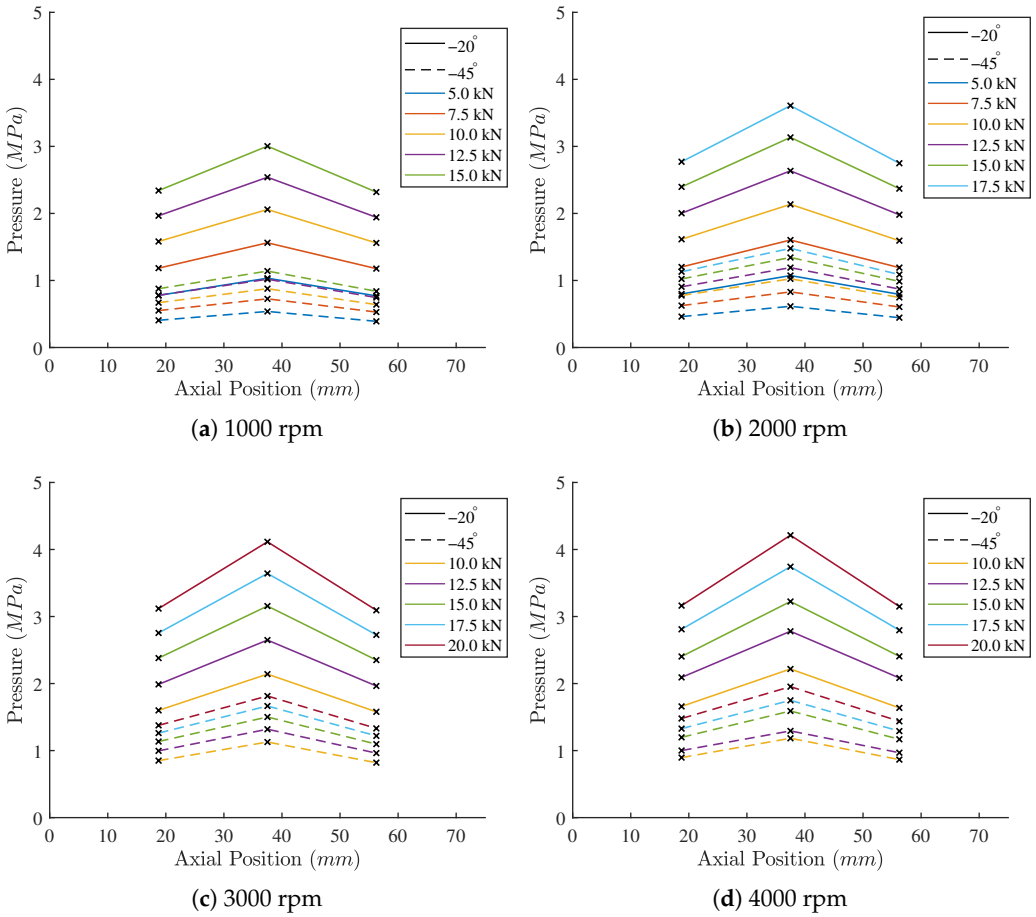

Figure 7. Axial pressure profiles at angular positions $-20°$ and $-45°$ at various rotational speeds.

Figure 8 shows the variation of relative pressure against the shaft rotational speed for a range of applied loads. The relative pressure is defined as the maximum pressure normalised to the load, W, over the projected area of the shaft, A. The maximum pressure is taken as the maximum in the experimental data, which is consistently the value measured at the $-20°$ location along the centreline. The relative pressure is reasonably constant across the experimental range, varying between 1.5 and 1.67. Increasing the rotational speed tends to increase the relative pressure with a difference of approximately 0.13 between 1000 rpm and 4000 rpm for all loads. The load tends to decrease the relative pressure linearly, with an approximately 0.08 difference between 7.5 kN and 20 kN.

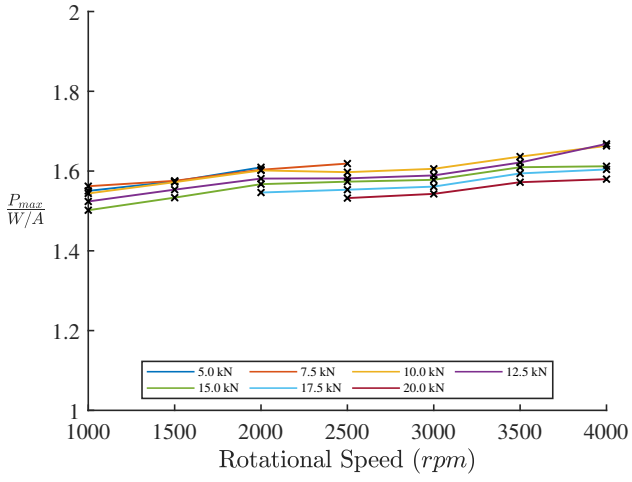

Figure 8. Maximum relative pressure against the rotational speed for varied loads.

Temperature profiles along the circumferential centreline near the film-bush interface are presented in Figure 9. It compares the speed effects at a range of constant loads. Qualitatively, a consistent profile is observable across the parameter range, where there is a temperature rise between the inlet and outlet. The shape of the profile reflects the general trend observed in full journal bearings, where the temperature rises to a peak downstream of the minimum film height. This is due to viscous dissipation and fluid convection. In a half-journal configuration, the classical 'cooling towards the outlet' can be truncated depending on load and fresh oil inflow. Indeed, in this configuration, this characteristic cooling profile appears to be truncated, and cooling towards the outlet of the lubrication region is less prevalent, except at the highest load in Figure 9d. The general magnitudes of temperature are more affected by the rotational speed in comparison to the applied load; for example, the change in the outlet temperature at 10 kN between 2000 rpm and 4000 rpm is approximately 11 °C, while the outlet temperature change at 4000 rpm between 10 kN and 20 kN is approximately 2 °C. This reflects the primary heat generation mechanism in the lubrication region as viscous dissipation. The applied load tends to have a greater effect on the profile shape, which can be seen by comparing the profiles at 10 kN, Figure 9b, and at 20 kN, Figure 9d.

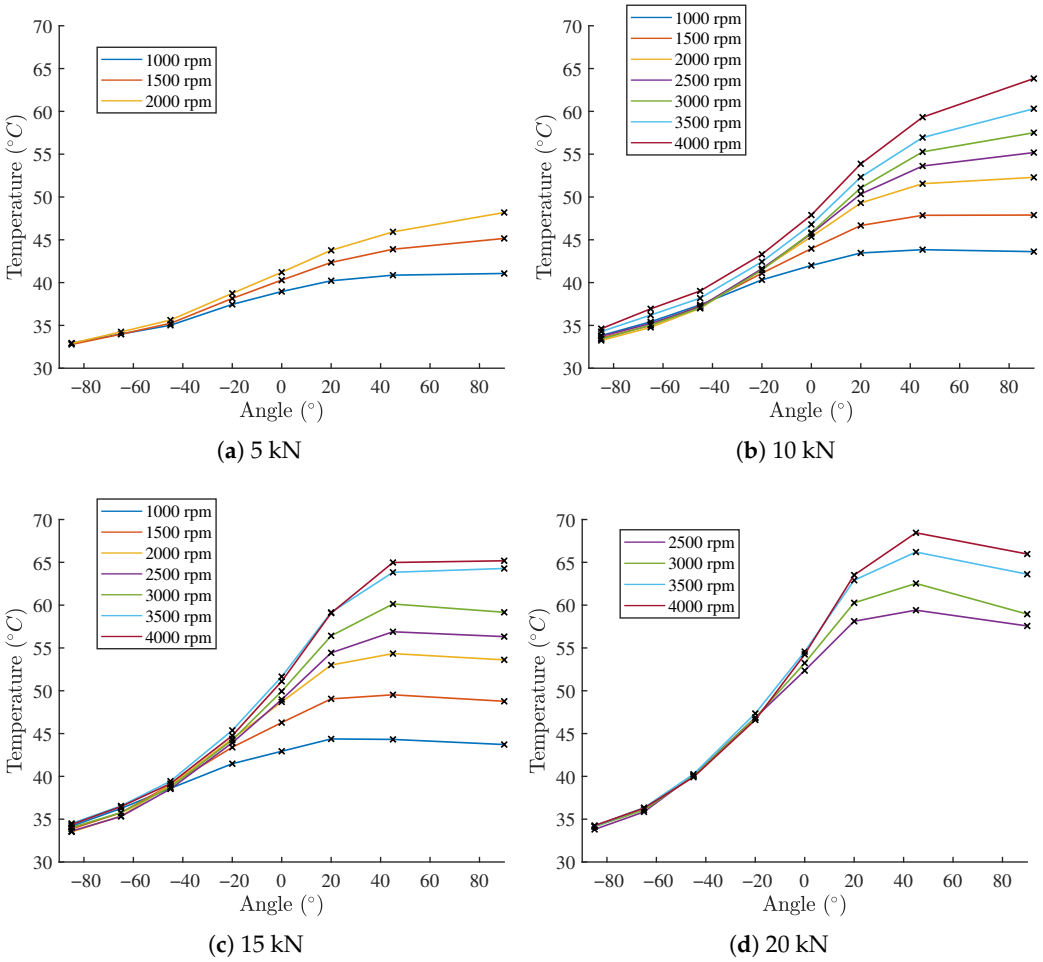

(**a**) 5 kN (**b**) 10 kN

(**c**) 15 kN (**d**) 20 kN

Figure 9. Effect of rotational speed at constant loads on the centreline temperature.

The temperature close to the inlet at the angular position −85° is very similar between the cases, approximately 34 ± 0.5 °C. This similarity could be due to the disconnection between the inlet and outlet of the film in the half-journal configuration compared to the full journal, where the lubricant is fed back into the contact region. The oil fed into the shaft-bush contact is therefore predominantly fresh oil at the fixed supply temperature. These

results highlight a potential advantage of the half-journal configuration, where the oil entering the lubrication region is closely controlled by the oil supply and is minimally affected by recirculating oil exiting the lubrication region, as in a traditional full-journal configuration.

The trend of the temperature profile near the outlet of the film at 90° tends to vary with the load, where the temperature gradient changes from positive at 5 kN in Figure 9a to negative at 20 kN in Figure 9b. This is further highlighted in Figure 10, which compares temperature profiles at a constant rotational speed of 3000 rpm for a varied applied load.

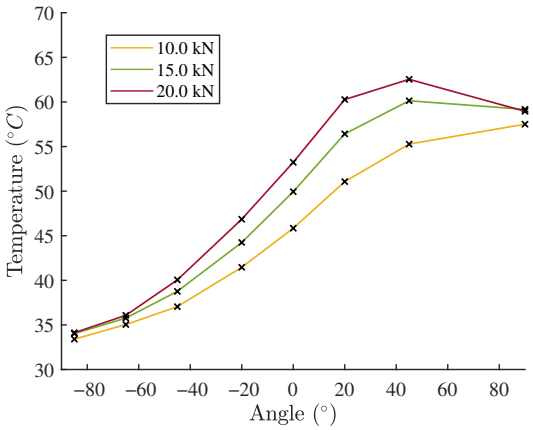

Figure 10. Centreline temperature profiles for varied loads at 3000 rpm.

Figure 11 shows a comparison of the maximum temperature change against the rotational speed with varied applied load. The maximum temperature change is calculated as the ratio of the maximum measured temperature along the centreline to the temperature measured nearest to the inlet at an angular position at −85°. A consistent trend is shown where the temperature change correlates positively with the rotational speed and applied load.

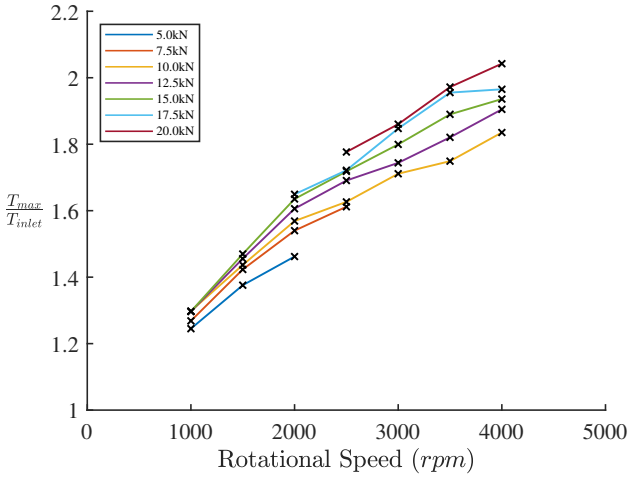

Figure 11. Temperature change between the inlet and the maximum against the rotational speed for varied loads.

The relation with the rotational speed appears to follow a logarithmic profile with a decreasing gradient as the rotational speed increases. This behaviour could be caused by the exponential viscosity-temperature relationship, which results in a lower viscosity at higher temperatures. The primary heat generation mechanism in the lubrication region is likely viscous heating caused by the high shearing of the fluid, and correlates with the viscosity of the oil. Therefore, the reduction in viscosity due to the higher temperature

will reduce the heat generated and will follow a similar trend to the viscosity-temperature behaviour, resulting in the logarithmic profile.

For each load, a non-dimensional temperature correlation is presented in the form of Equation (1), where W is the applied load (kN), and ω is the rotational speed (rpm).

$$\frac{T_{max}}{T_{inlet}} = a(W)log(\omega) + b(W) \quad (1)$$

The correlation is defined by two coefficients, a and b, which are dependent on the applied load. Figure 12 shows the results of the functional form required for each coefficient, which vary linearly with the applied load. The coefficient a has a positive gradient, Figure 12a, and b has a negative gradient, Figure 12b. These coefficients are then used in the final correlation for the temperature change in a half-journal configuration based on the rotational speed and applied load.

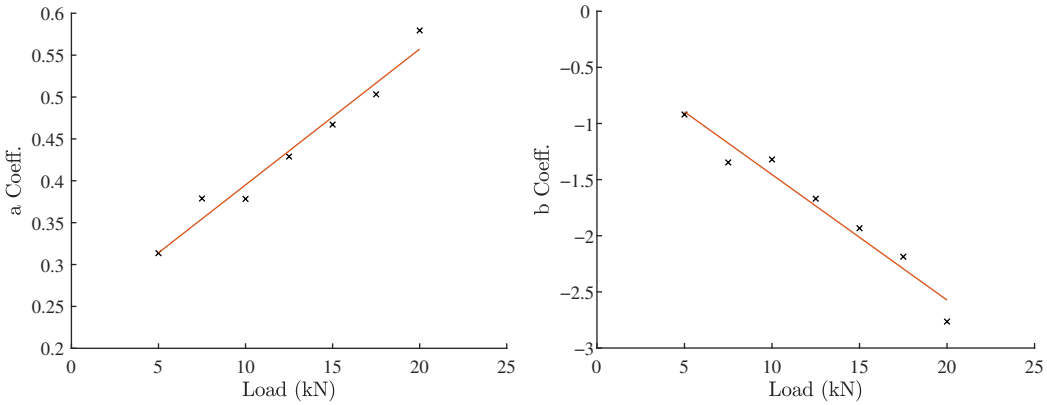

Figure 12. (**a**) Variation of the logarithmic correlation coefficient a against the applied load; (**b**) variation of the logarithmic correlation coefficient b against the applied load.

Figure 13 shows the results of fitting the temperature change to the original data set using the logarithmic correlation in Equation (1), and the linear correlation for the coefficients in Figure 12. The temperature change model shows good comparison with the data at higher rotational speeds. The correlation has a maximum difference from the data of 0.0318, with an average difference of 0.0151.

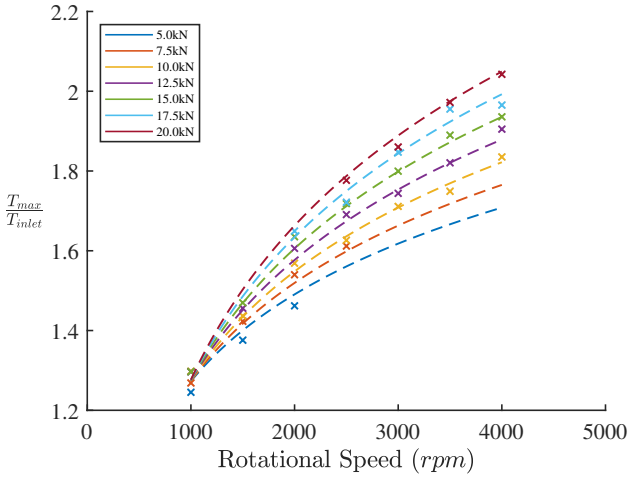

Figure 13. Temperature change between the inlet and the maximum against the rotational speed for varied loads compared to the implemented logarithmic predictive model.

The ultrasonic measurements provide profiles of film height in the lubrication region for each test case, as presented in Figure 14, which shows the mean film height profile of each test case. The shaded region is calculated from double the standard deviation to give a 95% confidence band.

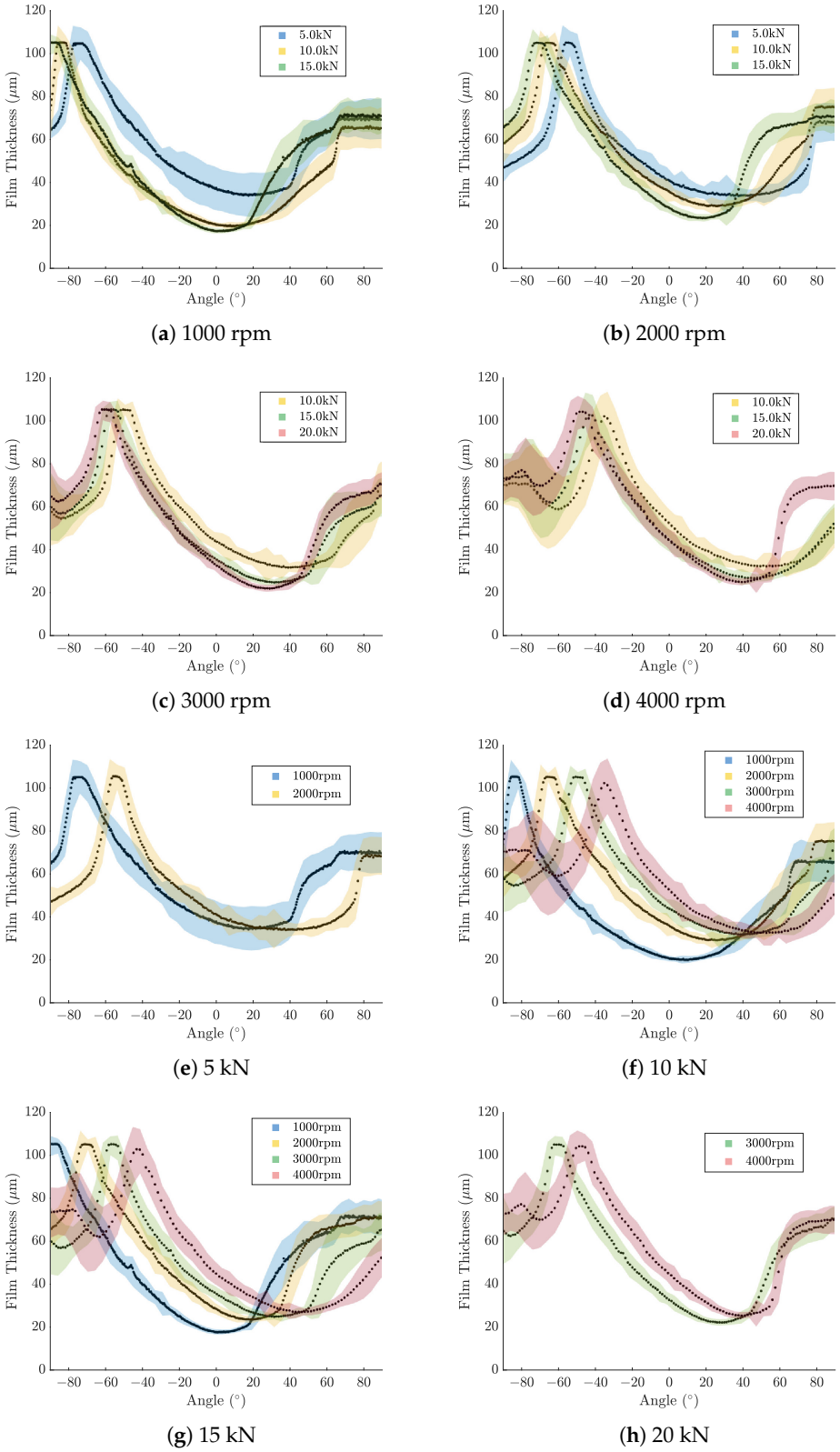

(**a**) 1000 rpm (**b**) 2000 rpm

(**c**) 3000 rpm (**d**) 4000 rpm

(**e**) 5 kN (**f**) 10 kN

(**g**) 15 kN (**h**) 20 kN

Figure 14. Profiles of film height with boundaries of two standard deviations for constant speeds (**a**–**d**) and constant load (**e**–**h**).

The profiles in Figure 14 can generally be separated into three regimes. The first regime is broadly in the range of $-90°$ to $-40°$, where the film height increases sharply to approximately 100 µm due to inlet effects caused by the oil feed. The second regime follows a parabolic profile down to the minimum film thickness and categorises the region of interest where the lubricating film forms. The parabolic profile is consistent with the expected parabolic shape for a journal-bearing-like geometry.

The third regime begins downstream of the minimum film thickness, where the film enters the diverging wedge. In this region, the measured profile deviates from the expected parabolic trend and exhibits a higher degree of uncertainty, as indicated by the larger shaded band in Figure 14. This behaviour is expected to be caused by cavitation, which forms when the local pressure in the diverging region falls below the lubricant saturation pressure. While explicit observation of cavitation is beyond the scope of this study, it is well known that cavitation alters the acoustic properties of the lubrication film. As a result, the returned ultrasonic signal becomes less stable, leading to increased variance in the inferred film thickness. This behaviour is consistent with the original study on ultrasonic measurements for lubricating films [11,13].

The variance in the film height profiles is generally low in the region of interest, the second regime surrounding the minimum film height. The uncertainty tends to increase at low load and rotational speed cases, which is shown particularly when comparing Figure 14a,b where the greatest variance is for the case at 5 kN and 1000 rpm. This behaviour could be attributed to greater instability at low rotational speed and load.

The general trend in the minimum film height is seen to decrease with increasing load and move closer to BDC at $0°$, which is consistent with the behaviour of full journal bearings. This trend can be seen in Figure 14a–d, which compare the film height profiles at fixed rotational speeds. Conversely, the film height tends to decrease and move further from BDC as the rotational speed increases, as shown in Figure 14.

The angular positions at which the minimum film thickness occurs for each rotational speed and load setting are presented in Figure 15, along with the magnitude of the minimum film height. The effect of rotational speed and load is clearly shown, where the rotational speed shifts the minimum further downstream, while the load shifts the minimum upstream. The load also appears to have a larger effect on the magnitude of the minimum compared to the rotational speed. The uncertainties are also shown, which are potentially due to cavitation-related signal disruption and local inlet effects. This is particularly relevant for the 15.0 kN load and 4000 rpm case, where there is a deviation in the minimum film thickness compared to the trend. This could be attributed to the interaction between cavitation and the measurement uncertainty. Nevertheless, the angular location at which this minimum film thickness occurs still follows the general trend.

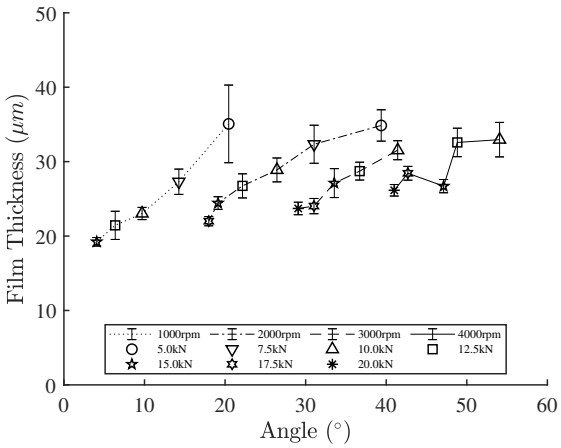

Figure 15. Angular positions of the minimum film height.

4. Conclusions

A half-journal bearing rig was developed to operate at rotational speeds ranging from 1000 to 4000 rpm, accommodating loads between 5 and 20 kN. It is equipped with instrumentation for comprehensive, simultaneous temperature, pressure, and film-thickness performance analysis. This work was motivated by the need for a comprehensive data set of journal bearing performance under realistic operating scenarios, including high loads, using detailed, synchronised measurements of key thermohydrodynamic parameters. The aim was to evaluate a well-lubricated journal bearing across a range of loads and speeds using a fully instrumented, high-load half-journal test platform, with the objective of capturing temperature, pressure, and film-thickness data to assess their variation with operating conditions.

Temperature sensors are embedded in both the shaft and the bearing bush to monitor thermal variations during operation. The rig also features pressure sensors strategically positioned to measure the lubricating film's pressure distribution, ensuring accurate data on load-bearing capacity. A novel aspect of the rig is its ultrasonic measurement setup, which allows precise, time- and cycle-averaged monitoring of the lubricating film thickness, providing detailed insights into the lubrication regime under various operational conditions.

Temperature measurements in both the shaft and bush followed expected trends, with gradual increases corresponding to higher loads and speeds. Pressure data within the lubricating film aligned with theoretical expectations, showing a stable pressure profile that correlated with load conditions. The ultrasonic film thickness measurements confirmed the presence of a full hydrodynamic lubrication regime across all tested conditions, with the film thickness decreasing as load increased, consistent with classical lubrication theory. The ultrasonic measurements reveal distinct film height profiles in the lubrication region, categorised into three regimes: a sharp increase from $-90°$ to $-40°$, a parabolic region around the minimum film height, and a region with higher uncertainty due to cavitation effects. The parabolic profile aligns with expected journal-bearing behaviour, while increased uncertainty at low loads and speeds, particularly at 5 kN and 1000 rpm, indicates greater instability in these conditions. Overall, the minimum film height decreases and shifts closer to the bottom dead centre as load increases, consistent with full journal bearing behaviour. Conversely, as rotational speed increases, the film height decreases and shifts further from the bottom dead centre. The analysis shows that load significantly impacts the magnitude of the minimum film height, more so than rotational speed, highlighting the critical role of load and speed in determining lubrication film characteristics. To complement future numerical investigations, temperature data were further analysed to develop a correlation linking rotational speed and load with the expected temperature rise due to viscous heating within the operating range tested, reported above. The correlation matches the non-dimensional temperature data to within an average of 0.0151.

These results validate the rig's reliability and accuracy for analysing journal bearing performance under a range of operational scenarios. Additionally, the integration of the ultrasonic circumferential film measurements with instrumented pressure and temperature measurements in a high-load half-journal platform with controlled inlet conditions allows the data set to be applied for numerical validation with well-defined boundaries.

Author Contributions: Conceptualization, J.L., H.M., B.C.R., S.A. and C.E.; methodology, J.L., H.M., B.C.R. and K.F.; software, J.L. and H.M.; validation, J.L., H.M., B.C.R. and S.A.; formal analysis, J.L., H.M., B.C.R. and S.A.; investigation, J.L., H.M., B.C.R. and S.A.; resources, C.E.; data curation, J.L. and H.M.; writing—original draft preparation, J.L., H.M., B.C.R. and S.A.; writing—review and editing, H.F., H.M., B.C.R. and S.A.; visualization, J.L. and H.M.; supervision, H.M., B.C.R., S.A. and C.E.; project administration, B.C.R., S.A. and C.E.; funding acquisition, C.E. All authors have read and agreed to the published version of the manuscript.

Funding: This research was funded by Rolls-Royce plc and the EPSRC through the Prosperity Partnership Grant "Cornerstone: Mechanical Engineering Science to Enable Aero Propulsion Futures" grant number EP/R004951/1.

Data Availability Statement: The original data presented in this study are openly available in Zenodo at [22].

Conflicts of Interest: The authors declare no conflict of interest.

References

1. Chen, Y.; Shi, X.; Wang, X.; Wang, H.; Yu, C.; Sun, Y. Results in Engineering Multi-objective analysis design of spiral groove conical bearing considering cavitation effects. *Results Eng.* **2022**, *15*, 100582. [CrossRef]
2. Zhang, J.; Han, D.; Song, M.; Xie, Z.; Rao, Z.; Zou, D. Theoretical and experimental investigation on the effect of supply pressure on the nonlinear behaviors of the aerostatic bearing-rotor system. *Mech. Syst. Signal Process.* **2021**, *158*, 107775. [CrossRef]
3. Hu, Y.; Meng, Y. Theoretical and Experimental Study of Transient Behavior of Spiral-Groove Thrust Bearings during Theoretical and Experimental Study of Transient Behavior of Spiral-Groove. *Tribol. Trans.* **2020**, *63*, 154–172. [CrossRef]
4. Tower, B. First Report on Friction Experiments. *Proc. Inst. Mech. Eng.* **1883**, *34*, 632–659. [CrossRef]
5. Stanton, T.E. On the characteristics of cylindrical journal lubrication at high values of the eccentricity. *Proc. R. Soc. London. Ser. A Contain. Pap. A Math. Phys. Character* **1922**, *102*, 241–255. [CrossRef]
6. Ma, M.T.; Taylor, C.M. An experimental investigation of thermal effects in circular and elliptical plain journal bearings. *Tribology* **1996**, *29*, 19–26. [CrossRef]
7. Syverud, T.; Tanaka, M. Experimental investigation of the effect of shaft heating and cooling on single bore journal bearing. *Wear* **1997**, *207*, 7481. [CrossRef]
8. Ferron, J.; Frene, J.; Boncompain, R. A Study of the Thermohydrodynamic Performance of a Plain Journal Bearing Comparison Between Theory and Experiments. *J. Lubr. Technol.* **1983**, *105*, 422–428. [CrossRef]
9. Costa, L.; Fillon, M.; Miranda, A.S.; Claro, J.C.P. An experimental investigation of the effect of groove location and supply pressure on the THD performance of a steadily loaded journal bearing. *J. Tribol.* **2000**, *122*, 227–232. [CrossRef]
10. Brito, F.P.; Miranda, A.S.; Bouyer, J.; Fillon, M. Experimental Investigation of the Influence of Supply Temperature and Supply Pressure on the Performance of a Two-Axial Groove Hydrodynamic Journal Bearing. *J. Tribol.* **2007**, *129*, 98–105. [CrossRef]
11. Dwyer-Joyce, R.S.; Drinkwater, B.W.; Donohoe, C.J. The measurement of lubricant-film thickness using ultrasound. *Proc. R. Soc. Ser. A Math. Phys. Eng. Sci.* **2003**, *459*, 957–976. [CrossRef]
12. Harper, P.; Hollingsworth, B.; Dwyer-Joyce, R.S.; Drinkwater, B.W. Journal Bearing Oil Film Measurement Using Ultrasonic Reflection. *Tribol. Ser.* **2004**, *41*, 469–476. [CrossRef]
13. Kasolang, S.; Dwyer-Joyce, R.S. Observations of film thickness profile and cavitation around a journal bearing circumference. *Tribol. Trans.* **2008**, *51*, 231–245. [CrossRef]
14. Niccolini, C.A.; Du, M.; Champ, H.; Stefani, F.; Silvestri, P. Experimental and Numerical Investigation about Small Clearance Journal Bearings under Static Load Conditions. *Adv. Tribol.* **2020**, *2020*, 8844879. [CrossRef]
15. Marey, N. Experimental Evaluation of the Effect of Oil Supply Pressure related to Marine Slow Speed Diesel Engine on Oil Film Pressure and Temperature Profiles within Journal Bearing. *Port-Said Eng. Res. J.* **2023**, *27*, 72–80. [CrossRef]
16. Van Der Meer, G.H.G.; Quinci, F.; Litwin, W.; Wodtke, M.; Van Ostayen, R.A.J. Experimental comparison of the transition speed of a hydrodynamic journal bearing lubricated with oil and magnetorheological fluid. *Tribol. Int.* **2023**, *189*, 108976. [CrossRef]
17. Cao, H.; Wu, R.; Chen, H.; Lu, C. An Experimental Investigation of the Thermohydrodynamic Performance of a Steady Loaded Hole-Entry Hybrid Journal Bearing. *IOP Conf. Ser. Mater. Sci. Eng.* **2019**, *491*, 012011. [CrossRef]
18. Eastman. Technical Data Sheet Eastman™ Turbo Oil 2197. 2024. Available online: https://www.eastman.com/en/products/product-detail/71097791/turbo-oil-2197 (accessed on 24 October 2025).
19. Reddyhoff, T.; Kasolang, S.; Dwyer-Joyce, R.; Drinkwater, B. The phase shift of an ultrasonic pulse at an oil layer and determination of film thickness. *Proc. Inst. Mech. Eng. Part J J. Eng. Tribol.* **2005**, *219*, 387–400. [CrossRef]
20. Dou, P.; Jia, Y.; Zheng, P.; Wu, T.; Yu, M.; Reddyhoff, T.; Peng, Z. Review of ultrasonic-based technology for oil film thickness measurement in lubrication. *Tribol. Int.* **2022**, *165*, 107290. [CrossRef]

21. Paleo Cageao, P.; Simmons, K.; Prabhakar, A.; Chandra, B. Assessment of the Oil Scoop Capture Efficiency in High Speed Rotors. *J. Eng. Gas Turbines Power* **2018**, *141*, 012401. [CrossRef]
22. Layton, J.; Medina, H.; Fadhila, H.; Rothwell, B.; Ambrose, S.; Farbrother, K.; Eastwick, C. Experimental Investigation of a Highly-Loaded Half-Journal Bearing. Dataset. 2026. Available online: https://zenodo.org/records/18375341 (accessed on 26 January 2026).

Disclaimer/Publisher's Note: The statements, opinions and data contained in all publications are solely those of the individual author(s) and contributor(s) and not of MDPI and/or the editor(s). MDPI and/or the editor(s) disclaim responsibility for any injury to people or property resulting from any ideas, methods, instructions or products referred to in the content.